Induction of altered mRNA expression profiles caused by fibrous and granular dust

SIMONE HELMIG[1], ELKE DOPP[2,3], SIBYLLE WENZEL[1], DIRK WALTER[1] and JOACHIM SCHNEIDER[1]

[1]Institute and Outpatient Clinic for Occupational and Social Medicine, Justus-Liebig University, D-35392 Giessen;
[2]Institute of Hygiene and Occupational Medicine, University of Duisburg-Essen, D-45122 Essen;
[3]Centre for Water and Environmental Research (ZWU), University of Duisburg-Essen, D-45141 Essen, Germany

Received April 17, 2013; Accepted October 2, 2013

DOI: 10.3892/mmr.2013.1765

Abstract. Natural and synthetic fibres and particles are being introduced into the workplace and environment daily. Comparative analyses of the induced signalling pathways are essential in order to understand the potential hazards of these particles. To identify the molecular characteristics of particles and fibres, we selected crocidolite and chrysotile asbestos as representatives for fibered dust and titanium dioxide (TiO_2) (100-200 nm), zirconium dioxide (ZrO_2) (50-100 nm) and hematite (Fe_2O_3) (20 nm) as representatives for bio-persistent granular dust. SV-40 virus-transformed human bronchial epithelial cells (BEAS-2B) were exposed to well-defined fibres and particles. RT^2 Profiler™ PCR Array Human Stress & Toxicity PathwayFinder was used to compare the relative mRNA expression of 84 genes. A detailed characterization of the dust samples used in this study was accomplished to ensure comparability to other studies. Investigation of mRNA expression of 84 signalling molecules attributed to pathways such as DNA damage and repair; oxidative/metabolic stress; growth arrest and senescence; inflammation, proliferation and carcinogenesis; and heat shock and apoptosis revealed that crocidolite and chrysotile asbestos induced mRNA expression of pathway molecules involved in proliferation and carcinogenesis, as well as inflammation. Titanium dioxide, zirconium dioxide and hematite mainly induced pathway molecules responsible for oxidative/metabolic stress and inflammation. Our findings suggest that the hazards of fibered dust mainly include the induction of direct toxicity by altering signalling pathways such as carcinogenesis and proliferation, while granular dust shows indirect toxicity by altering signalling pathways involved in inflammatory processes. PCR arrays, therefore, may be a helpful tool to estimate the hazard risk of new materials.

Correspondence to: Dr Simone Helmig, Institute and Outpatient Clinic for Occupational and Social Medicine, Justus-Liebig University, Aulweg 129, D-35392 Giessen, Germany
E-mail: simone.helmig@arbmed.med.uni-giessen.de

Key words: crocidolite, chrysotile, titanium dioxide, zirconium dioxide, hematite, human stress and toxicity pathway, screening tests

Introduction

Human populations are exposed to environmental and occupational fibrous and granular dust. The number of synthetic or natural fibres and particles being introduced into the environment is continuously increasing. Due to the increasing number and compositional heterogeneity of potentially harmful fibres and particles, there is a crucial need to understand the mechanisms of their pathogenicity.

Lately, nano-sized particles with a diameter below 100 nm have become the focus of attention, as they are predicted to have a higher toxic potential as a result of their high surface/mass ratios. However, the crystalline structure, surface properties, solubility and particle size are also known to be relevant parameters (1). Therefore an accurate characterization of the particles is essential to allow an interpretation of the results of a study.

It is reasonable to categorise particles and fibres by their molecular effects. To identify the molecular characteristics of particles and fibres we used Union Internationale Contre le Cancer (UICC) crocidolite and chrysotil asbestos as fibered dust and titanium dioxide (TiO_2) as well as zirconium dioxide (ZrO_2) as representatives for bio-persistent granular dust. Hematite (Fe_2O_3) represents a nano-sized ultrafine dust with an iron (Fe) content of ~70%. Asbestos is known to be a carcinogen associated with the induction of lung cancer, mesothelioma and lung fibrosis (2). DNA damage and apoptosis are important downstream effects of asbestos, which occur in all the major lung target cells studied (3). Exposure to asbestos fibres causes alterations in cell signalling (4) and induction of various pro-inflammatory molecules, such as cytokines (5,6). The pathogenicity of various types of asbestos fibres is thought to be associated with fibre size, geometry and surface composition (7). The iron content in particular has to be considered when assessing the toxicity of asbestos fibres. Crocidolite ($Na_2[Fe^{3+}]_2[Fe^{2+}]_3Si_8O_{22}[OH]_2$) typically has a high iron content of ~26%, while the iron content in chrysotile ($Mg_6Si_4O_{10}[OH]_8$) ranges between 1 and 6%, and is primarily present as a surface contaminant (8).

In order to verify that the evoked effects are not only due to the iron content of the investigated particles, we used hematite with an iron content of ~70%. Hematite, the hexagonal modification of iron (III) oxide (α-Fe_2O_3) is the most important industrial iron oxide used.

Titanium dioxide, also known as titanium (IV) oxide, is the naturally occurring oxide of titanium, which is commercially used in a wide range of products, such as paint, varnishes, paper coating and cosmetics (9,10). Micro-sized titanium dioxide is suggested to be biologically inert (11,12), although an inflammatory response has been described (10). Particles can generate reactive oxygen species; particularly in the case of nano-sized particles, DNA adducts are observed in human lung cells (9,13). Additionally, increased micronucleus formation and DNA breakage, as well as activation of DNA damage checkpoint kinases in nano-TiO_2-treated lymphocytes, have been demonstrated (14).

Zirconium dioxide, also known as zirconia, is used in various products, such as ceramic materials, scratch resistant varnishes and coatings, as well as in medical implants (15,16).

The aim of this study was to compare the effects of well-defined fibres (UICC, crocidolite and chrysotile 'A') and different size particles (titanium dioxide, zirconium dioxide and hematite) on human bronchial epithelial cells (BEAS-2B). We focused on the mRNA expression of 84 signalling molecules attributed to pathways such as 'DNA damage and repair', 'oxidative/metabolic stress', 'growth arrest and senescence', 'inflammation', 'proliferation and carcinogenesis', 'heat shock' and 'apoptosis'.

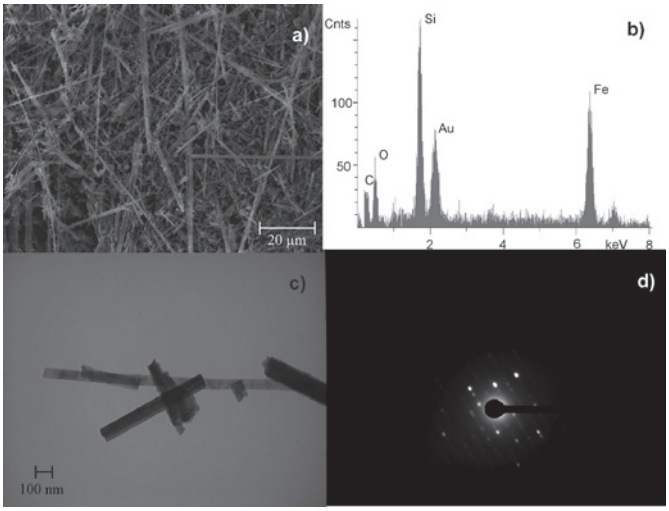

Figure 1. Union Internationale Contre le Cancer (UICC) crocidolite asbestos fibres. (a) Scanning electron microscopy (SEM) (magnification, x1,000), (b) energy dispersive X-ray (EDX)-analysis, (c) transmission electron microscopy (TEM) (magnification, x40,000) and (d) electron diffraction pattern.

Materials and methods

Materials. Crocidolite asbestos (UICC, South African NB #4173-111-3) and chrysotil asbestos (UICC, Rhodesian NB #4173-11-2) were used as standard references for bio-persistent fibrous dust. Titanium dioxide anatase (Sigma-Aldrich Chemie GmbH, Steinheim, Germany; AL232033) and zirconium dioxide (Sigma-Aldrich Chemie GmbH; AL230693) represented bio-persistent granular dust. Hematite, α-Fe_2O_3 (Nanopowder 544884, Sigma-Aldrich Chemie GmbH) was used to represent ultrafine particles.

Characterization of dust materials. For a detailed description of the characterization method, refer to a former paper (17). Scanning electron microscopy (SEM; Hitachi S-2700, Chiyoda, Japan) was used to identify particle geometry as well as the microstructure of the samples. The element analysis resulted from energy dispersive X-ray (EDX). To optimize the conductivity (electron beam), all samples were deposited with a very fine gold (Au) layer using a sputtering technique. Transmission electron microscopy (TEM) analysis combined with electron diffraction (detection of crystallinity) was performed using a transmission electron microscope H-600 (Hitachi, Japan). Thermogravimetry (TG) measurements (corundum crucibles, heating rate 5 K/min and synthetic air atmosphere) for controlling impurities such as water were conducted using a thermo balance TG 209 F1 Iris (NETZSCH-Gerätebau GmbH, Selb, Germany).

Culture conditions. SV-40 virus-transformed BEAS-2B cells were obtained from the European collection of cell cultures (ECCC, 95102433). Approximately 10 million cells ($10x10^6$) after trypsinization and counting using a haemocytometer were plated in 75 cm^2 flasks (Falcon; Franklin Lakes, NJ, USA). The cells were grown in 15 ml Gibco® RPMI 1640 media containing 10-15% fetal calf serum (FCS), 0.5% gentamycin, 1% L-glutamine and 1% amphotericin. The cultures were maintained at 37˚C and 5% CO_2. After a 24-h pre-incubation, the cells were exposed to crocidolite (5 $\mu g/cm^2$), chrysotil (1 $\mu g/cm^2$), zirconium dioxide (10 $\mu g/cm^2$), titanium dioxide (10 $\mu g/cm^2$) or hematite (10 $\mu g/cm^2$) for 48 h. Unexposed cells served as negative controls. All experiments were repeated 4 times. Cytotoxicity and genotoxicity analyses were investigated intensively in various cell systems for crocidolite and chrysotile (18-21), titanium dioxide (22,23) and hematite (22,24). Based on the results of the above study, the particle concentrations did not show any loss of viability in the BEAS-2B cell line. Additionally, the same concentrations and incubation times were used in numerous published studies and therefore the results are comparable.

mRNA extraction and reverse transcription. After washing twice with PBS (37˚C), cells were trypsinized for ~30 sec with 10 ml of 0.05% trypsin and incubated for 10 min in 37˚C. Detached cells then were resuspended in 5 ml ice-cold PBS and centrifuged at 400 x g (without brakes) for 10 min in 15-ml centrifuge tubes. This step was repeated with 1 ml of ice-cold PBS in 1.5 ml Eppendorf tubes. mRNA was extracted immediately with RNeasy Mini kit® (Qiagen, Hilden, Germany) in accordance with the manufacturer's instructions. Reverse transcription was accomplished with the RT^2 First Strand kit (Qiagen) as suggested by the manufacturer.

RT^2 Profiler PCR Arrays®. The RT^2 RNA QC PCR Array® (SaBiosciences, Qiagen) was used to test for RNA quality and inhibitors of RT-PCR analyses. For quantitative comparison of mRNA levels, real-time PCR was performed using RT^2 Profiler PCR Arrays® Human Stress & Toxicity PathwayFinder PCR Array® (SaBiosciences). For each condition, four assays were carried out as independent samples. Gene expression was related to the mean expression of β_2 microglobulin (B2M) and hypoxanthine phosphoribosyltransferase 1 (HPRT) as house-

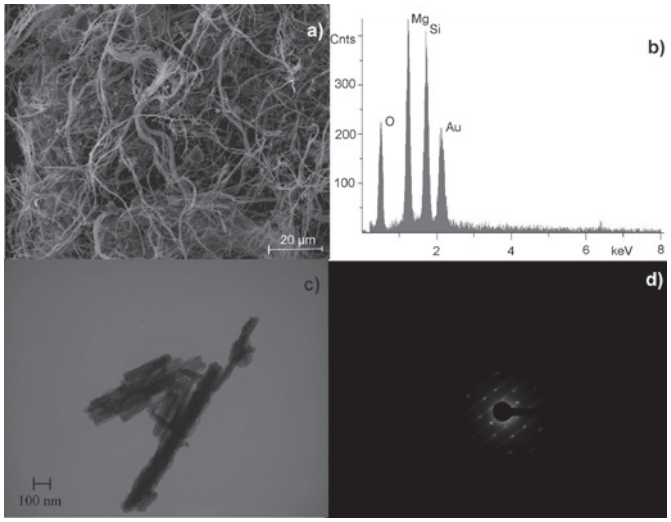

Figure 2. Union Internationale Contre le Cancer (UICC) chrysotile asbestos fibres. (a) Scanning electron microscopy (SEM) (magnification, x1,000), (b) energy dispersive X-ray (EDX) analysis, (c) transmission electron microscopy (TEM) (magnification, x40,000) and (d) electron diffraction pattern.

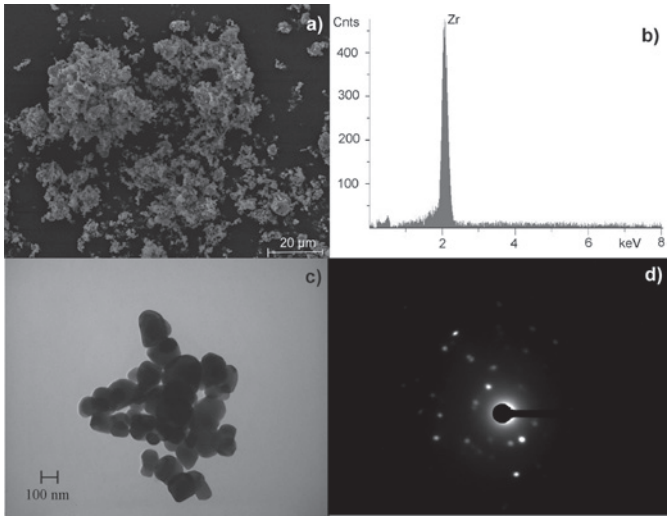

Figure 4. Crystalline zirconium dioxide (ZrO_2) aggregates. (a) Scanning electron microscopy (SEM) (magnification, x1,000), (b) energy dispersive X-ray (EDX)-analysis, (c) transmission electron microscopy (TEM) (magnification, x40,000) and (d) electron diffraction pattern.

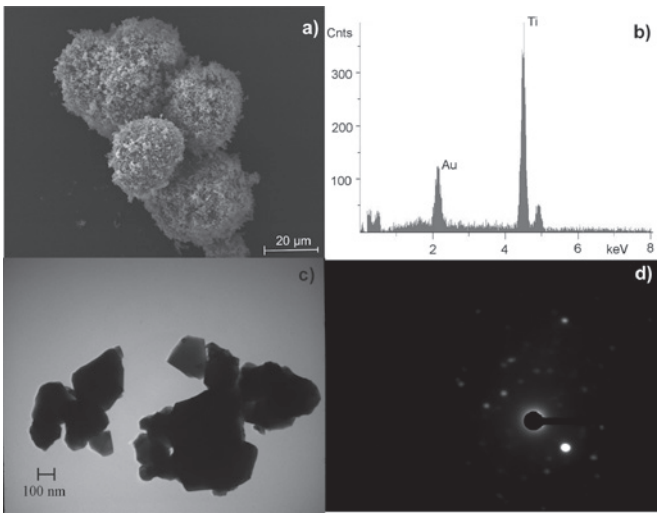

Figure 3. Irregularly shaped crystalline titanium dioxide (TiO_2) aggregates. (a) Scanning electron microscopy (SEM) (magnification, x1,000), (b) energy dispersive X-ray (EDX) analysis, (d) transmission electron microscopy (TEM) (magnification, x40,000) and (d) electron diffraction pattern.

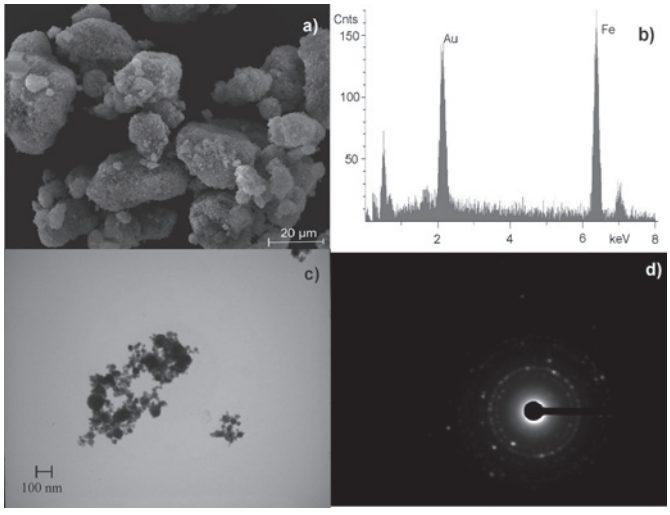

Figure 5. Agglomerates and aggregates of crystalline nano-sized hematite. (a) Scanning electron microscopy (SEM) (magnification, x1,000), (b) energy dispersive X-ray (EDX) analysis, (c) transmission electron microscopy (TEM) (magnification, x40,000) and (d) electron diffraction pattern.

keeping genes, since these were the two most stable of the five housekeeping genes included in the array. Only Ct values <35 were included in the calculations.

Statistical analysis. Calculations of expression were performed with the $2^{-\Delta\Delta CT}$ method according to Pfaffl (25). For analysis the PCR Array Data Analysis Software (Excel & Web-based) provided by SaBiosciences was used. The cut-off was set to CT>35. The P-values are calculated based on a Student's t-test of the replicate $2^{-\Delta Ct}$ values for each gene in the control and treatment groups. Results are shown as the mean of four samples for each condition in relation to the mean of four control samples. All statistical analyses were performed using the statistical software package, SPSS, 17.0 (SPSS, Inc., Chicago, IL, USA). P<0.05 was considered to indicate a statistically significant difference.

Results

Characterization of dust samples. UICC crocidolite South African ($Na_2(Fe_3^{2+}Fe_2^{3+}[(OH)_2|Si_8O_{22}]$) was shown to have 3,800 fibres/ml at a length of >5 μm and a diameter of <3 μm. The length to diameter ratio was at least 3:1 (WHO fibres). Crocidolite is a rigid and rod-like fibre with characteristic iron content (Fig. 1). Gold (Au) was detected in all EDX analyses due to the sputtering preparation technique.

UICC chrysotile 'A' Rhodesian ($Mg_6[(OH)_8|Si_4O_{10}]$) was shown to have 200 fibres/ml at a length of >5 μm and a diameter of <3 μm. The length to diameter ratio was at least

Table I. Relative mRNA expression of 84 genes after incubation of fibrous and granular dust in bronchial epithelial cells (BEAS-2B).

			Control group		Crocidolite		Chrysotile		ZrO_2		TiO_2		Hematite	
Pathway	Symbol	Refseq	AVG Ct	± SD	AVG Ct	± SD	AVG Ct	± SD	AVG Ct	± SD	AVG Ct	± SD	AVG Ct	± SD
Apoptosis signalling	ANXA5	NM_001154	20.94	0.18	21.15	0.28	20.96	0.49	21.26	0.92	21.33	0.58	21.04	0.31
	BAX	NM_004324	23.24	0.18	23.52	0.11	23.45	0.51	23.83	0.63	23.76	0.41	23.59	0.41
	BCL2L1	NM_138578	26.37	0.33	26.29	0.21	26.55	0.29	26.85	0.16	27	0.33	27.41	1.36
	CASP1	NM_033292	25.53	0.24	25.75	0.19	25.66	0.45	25.59	0.46	25.94	0.62	25.64	0.35
	CASP10	NM_001230	30.54	0.34	30.76	0.39	30.61	0.54	31.16	0.72	30.92	0.52	30.86	0.60
	CASP8	NM_001228	29.59	0.18	29.36	0.40	29.34	0.58	29.84	0.47	29.67	0.80	29.22	0.53
	FASLG	NM_000639	35	0.00	35	0.00	35	0.00	35	0.00	35	0.00	35	0.00
	NFKBIA	NM_020529	23.25	0.27	23.57	0.27	23.52	0.43	23.28	0.54	23.67	0.56	23.03	0.33
	TNF	NM_000594	35	0.01	35	0.00	34.99	0.03	34.76	0.26	35	0.00	34.70	0.60
	TNFRSF1A	NM_001065	23.27	0.28	23.56	0.25	23.33	0.38	23.38	0.60	24.02	0.61	23.33	0.38
	TNFSF10	NM_003810	27.03	0.24	27.70	0.39	27.58	0.30	27.81	1.02	28.21	0.59	27.59	0.52
DNA damage and repair	ATM	NM_000051	29.32	0.09	29.36	0.36	29.45	0.34	29.68	0.25	29.75	0.47	29.69	0.89
	CHEK2	NM_007194	26.51	0.27	27.03	0.28	27.02	0.53	27.04	0.36	27.36	0.49	26.99	0.54
	DDB1	NM_001923	24.18	0.21	24.27	0.27	24.59	0.37	24.81	0.28	24.71	0.40	24.75	0.84
	ERCC1	NM_001983	24.71	0.36	24.80	0.19	24.82	0.56	25.33	0.72	25.23	0.41	25.04	1.00
	ERCC3	NM_000122	26.25	0.40	26.37	0.26	26.43	0.46	26.88	0.65	26.72	0.43	26.58	1.03
	RAD23A	NM_005053	24.74	0.34	25.04	0.23	25.19	0.47	25.63	1.11	25.39	0.34	24.90	0.68
	RAD50	NM_005732	28.39	0.56	28.66	0.39	28.93	0.51	29.54	0.71	29.10	0.71	29.07	1.36
	UGT1A4	NM_007120	35	0.00	35	0.00	35	0.00	35	0.00	35	0.00	35	0.00
	UNG	NM_003362	24.48	0.25	24.74	0.14	24.80	0.26	24.70	0.35	25.07	0.37	24.68	0.21
	XRCC1	NM_006297	24.90	0.38	25.29	0.21	25.38	0.45	25.52	0.62	25.70	0.35	25.19	0.54
	XRCC2	NM_005431	26.83	0.20	27.43	0.75	27.16	0.43	27.63	0.56	27.55	0.26	27.23	0.69
Growth arrest and senescence	CDKN1A	NM_000389	21.32	0.20	21.80	0.15	21.79	0.61	21.62	0.47	22.22	0.41	21.61	0.13
	DDIT3	NM_004083	24.77	0.10	25.05	0.23	25.04	0.51	25.18	0.63	25.08	0.36	24.68	0.36
	GADD45A	NM_001924	26.80	0.40	26.90	0.28	26.99	0.55	27.29	0.71	27.44	0.53	26.85	0.68
	GDF15	NM_004864	22.93	0.10	23.08	0.09	23.21	0.38	23.41	0.59	23.56	0.52	23.01	0.17
	IGFBP6	NM_002178	23.26	0.21	23.72	0.14	23.55	0.60	23.97	0.78	23.94	0.46	23.74	0.77
	MDM2	NM_002392	22.95	0.23	23.40	0.25	23.49	0.48	23.53	0.38	23.92	0.26	23.73	0.82
	TP53	NM_000546	23.63	0.40	24.03	0.19	24.03	0.40	24.69	1.18	24.49	0.33	24.24	0.98
Heat shock	DNAJA1	NM_001539	22.66	0.30	23.08	0.28	23.06	0.39	23.25	0.64	23.06	0.61	22.84	0.56
	DNAJB4	NM_007034	25.19	0.37	25.41	0.32	25.61	0.49	25.83	0.32	25.85	0.38	25.63	0.84
	HSF1	NM_005526	23.21	0.28	23.62	0.26	23.48	0.50	23.73	0.74	23.66	0.71	22.89	0.27
	HSPA1A	NM_005345	22	0.20	22.27	0.24	22.17	0.47	22.29	0.46	22.53	0.65	21.95	0.34

Table I. Continued.

Pathway	Symbol	Refseq	Control group		Crocidolite		Chrysotile		ZrO_2		TiO_2		Hematite	
			AVG Ct	± SD	AVG Ct	± SD	AVG Ct	± SD	AVG Ct	± SD	AVG Ct	± SD	AVG Ct	± SD
Heat shock	HSPA1L	NM_005527	30.30	0.37	30.63	0.15	30.51	0.46	31.09	0.71	30.60	0.51	30.45	0.51
	HSPA2	NM_021979	25.13	0.13	25.48	0.24	25.49	0.32	25.58	0.47	26.09	0.50	25.57	0.09
	HSPA4	NM_002154	25.53	0.35	25.92	0.19	25.92	0.48	26.15	0.24	26.19	0.39	25.94	0.62
	HSPA5	NM_005347	26.45	0.18	26.39	0.30	26.36	0.37	26.50	0.22	26.24	0.47	25.93	0.21
	HSPA6	NM_002155	34.11	0.37	34.13	0.47	34.25	0.25	34.31	0.60	34.17	0.58	33.75	0.47
	HSPA8	NM_006597	21.29	0.30	21.70	0.23	21.70	0.57	21.97	0.44	21.87	0.48	21.69	0.63
	HSPB1	NM_001540	20.63	0.31	21.23	0.30	21.15	0.57	21.27	0.61	21.32	0.62	20.69	0.28
	HSP90AA2	NM_001040141	27.19	0.37	27.58	0.34	27.35	0.58	27.51	0.56	27.37	0.87	26.63	0.24
	HSP90AB1	NM_007355	20.68	0.37	22.64	2.85	21.25	0.61	21.18	0.49	21.35	0.58	20.77	0.39
	HSPD1	NM_002156	22.56	0.40	22.93	0.27	22.73	0.55	23.14	0.67	23.20	0.51	22.61	0.49
	HSPE1	NM_002157	21.75	0.24	22.05	0.44	21.88	0.44	22.26	0.44	22.21	0.63	21.64	0.25
	HSPH1	NM_006644	25.70	0.40	26.12	0.44	25.89	0.59	26.31	0.57	25.96	0.79	25.54	0.26
Inflammation	CCL21	NM_002989	35	0.00	35	0.00	35	0.00	35	0.00	35	0.00	35	0.00
	CCL3	NM_002983	33.94	0.25	33.55	0.54	32.94	0.58	34.04	0.50	33.27	0.33	33.34	1.12
	CCL4	NM_002984	35	0.00	35	0.00	35	0.00	35	0.00	35	0.00	35	0.00
	CSF2	NM_000758	30.44	0.22	30.46	0.26	30.46	0.39	30.74	0.99	30.79	0.68	30.15	0.35
	CXCL10	NM_001565	34.55	0.55	35	0.00	34.69	0.42	35	0.00	34.96	0.08	35	0.00
	IL18	NM_001562	24.38	0.22	24.89	0.27	24.93	0.77	25.16	0.87	25.18	0.39	24.58	0.36
	IL1A	NM_000575	28.48	0.25	28.70	0.18	28.75	0.53	29.04	0.55	29.23	0.34	28.77	0.76
	IL1B	NM_000576	27.65	0.29	27.83	0.28	27.95	0.56	28.35	0.75	28.51	0.41	27.84	0.45
	IL6	NM_000600	26.89	0.31	26.73	0.25	26.88	0.46	27.37	0.66	27.43	0.53	26.62	0.39
	LTA	NM_000595	34.47	0.50	34.62	0.51	34.28	0.83	34.75	0.43	34.77	0.14	34.26	0.12
	MIF	NM_002415	18.60	0.03	18.95	0.31	18.83	0.45	18.94	0.42	19.24	0.47	18.61	0.35
	NFKB1	NM_003998	23.72	0.28	24.17	0.35	23.97	0.28	23.97	0.49	24.51	0.56	23.75	0.28
	NOS2	NM_000625	33	0.43	33.20	0.21	32.93	0.50	33.23	0.92	33.20	0.76	32.88	0.14
	SERPINE1	NM_000602	25.42	0.18	25.53	0.29	25.56	0.39	25.80	0.32	25.77	0.35	25.22	0.58
Oxidative or metabolic stress	CAT	NM_001752	25.52	0.24	25.48	0.12	25.52	0.43	25.80	0.52	26.03	0.49	25.90	0.55
	CRYAB	NM_001885	29.21	0.43	29.88	0.53	29.75	0.83	29.80	1.10	30.21	1.05	29.32	0.22
	CYP1A1	NM_000499	33.09	0.38	33.30	0.35	33.20	0.49	33.14	0.56	33.31	0.51	32.97	0.19
	CYP2E1	NM_000773	33.96	0.30	34	0.48	34.13	0.53	34.09	0.79	34.22	0.44	34.16	0.63
	CYP7A1	NM_000780	35	0.00	34.92	0.16	35	0.00	35	0.00	35	0.00	35	0.00
	EPHX2	NM_001979	33.73	0.44	33.76	0.46	33.78	1.11	34.41	0.59	33.65	0.60	33	0.25
	FMO1	NM_002021	35	0.00	35	0.00	35	0.00	35	0.00	35	0.00	35	0.00
	FMO5	NM_001461	30.80	0.37	31.13	0.33	31.26	0.57	31.56	0.46	31.86	0.54	31.55	0.72

Table I. Continued.

			Control group		Crocidolite		Chrysotile		ZrO_2		TiO_2		Hematite	
Pathway	Symbol	Refseq	AVG Ct	± SD	AVG Ct	± SD	AVG Ct	± SD	AVG Ct	± SD	AVG Ct	± SD	AVG Ct	± SD
Oxidative or metabolic stress	GPX1	NM_000581	19.95	0.20	20.54	0.34	20.44	0.58	20.70	0.81	20.76	0.51	19.90	0.42
	GSR	NM_000637	28.92	0.54	28.85	0.37	29.13	0.36	29.15	0.12	28.92	0.43	28.89	0.95
	GSTM3	NM_000849	28.58	0.41	29.26	0.53	29.31	0.66	29.31	0.37	29.50	0.61	29.01	0.52
	HMOX1	NM_002133	23.13	0.23	23.60	0.39	23.63	0.59	23.80	0.75	23.40	0.64	22.63	0.46
	MT2A	NM_005953	17.82	0.15	18.12	0.39	18.03	0.24	18.01	0.56	18.26	0.53	17.71	0.27
	POR	NM_000941	27.09	0.42	27.38	0.32	27.29	0.64	28.10	0.87	27.80	0.34	27.36	0.95
	PRDX1	NM_002574	25.53	0.11	25.83	0.38	25.68	0.42	25.94	0.41	26.04	0.54	25.66	0.44
	PRDX2	NM_005809	23.35	0.29	23.80	0.26	23.64	0.54	24.03	0.81	24.07	0.19	23.67	0.75
	PTGS1	NM_000962	30.79	0.30	31.16	0.34	31.17	0.52	30.95	0.63	31.46	0.52	30.85	0.31
	SOD1	NM_000454	20.90	0.25	21.32	0.25	21.35	0.21	21.10	0.29	21.62	0.38	21.01	0.24
	SOD2	NM_000636	22.73	0.45	23	0.18	23.07	0.44	23.10	0.32	23.49	0.38	23.02	0.59
Proliferation and carcinogenesis	CCNC	NM_005190	24.85	0.42	24.74	0.20	24.83	0.35	24.72	0.34	24.93	0.63	25.24	0.97
	CCND1	NM_053056	29.24	0.24	29.24	0.33	28.98	0.36	29.68	0.52	28.82	0.66	28.97	0.88
	CCNG1	NM_004060	22.22	0.16	22.59	0.38	22.57	0.49	22.63	0.47	22.87	0.65	22.53	0.29
	E2F1	NM_005225	26.93	0.44	27.20	0.32	27.42	0.46	27.56	0.23	27.84	0.23	27.90	1.36
	EGR1	NM_001964	25.11	0.63	25.33	0.37	25.46	0.60	25.69	0.29	26.20	0.53	25.54	0.98
	PCNA	NM_182649	20.89	0.24	21.30	0.40	21.14	0.54	21.44	0.85	21.50	0.50	21.12	0.60
HSK	B2M	NM_004048	19.20	0.40	19.90	0.23	19.97	0.54	19.87	0.62	20.10	0.63	19.54	0.50
	HPRT1	NM_000194	23.14	0.25	23.73	0.25	23.68	0.43	23.69	0.48	23.86	0.61	23.47	0.30

Average and standard deviation of the Ct values of each gene are presented. ZrO_2, zirconium dioxide; TiO_2, titanium dioxide; HSK, housekeeping genes.

Table II. Comparing mRNA expression (95% CI) of DNA damage and repair molecules.

DNA damage and repair	Crocidolite fold change (95% CI)	Chrysotile fold change (95% CI)	Titanium dioxide fold change (95% CI)	Zirconium dioxide fold change (95% CI)	Hematite fold change (95% CI)
ATM	1.53[a] (1.07-1.98)	-	-	-	-
CHEK2	-	-	-	-	-
DDB1	1.48[a] (1.19-1.76)	-	-	-	-
ERCC1	1.47[a] (1.18-1.76)	1.46[a] (1.10-1.83)	-	-	-
ERCC3	1.44[a] (1.21-1.68)	1.39[a] (1.14-1.64)	-	-	-
RAD23A	1.27[a] (1.06-1.48)	-	-	-	-
RAD50	1.29[b] (1.03-1.57)	-	-	-1.45[c] [-1.19-(-1.85)]	-
UGT1A4	-	-	-	-	-
UNG	1.31[a] (1.13-1.49)	-	-	1.31[a] (1.04-1.58)	-
XRCC1	1.20[a] (1.07-1.34)	-	-	-	-
XRCC2	-	1.26[a] (1.04-1.47)	-	-	-

[a]P<0.050, [b]P<0.055 and [c]P=0.038. CI, confidence interval.

Table III. Comparing mRNA expression (95% CI) of oxidative and metabolic stress molecules.

Oxidative or metabolic stress	Crocidolite fold change (95% CI)	Chrysotile fold change (95% CI)	Titanium dioxide fold change (95% CI)	Zirconium dioxide fold change (95% CI)	Hematite fold change (95% CI)
CAT	1.62[a] (1.25-1.99)	1.58[a] (1.15-2.01)	-	-	-
CRYAB	-	-	-	-	-
CYP1A1	1.35[a] (1.07-1.63)	-	-	1.47[a] (1.18-1.76)	1.37[b] (1.01-1.72)
CY	-	-	-	-	-
CYP7A1	-	-	-	-	-
EPHX2	1.53[a] (1.01-1.72)		-	-	2.09[a] (1.12-3.05)
FMO1	-	-	-	-	-
FMO5	-	-	-	-	-
GPX1	-	-	-	-	-
GSR	1.64[a] (1.11-2.18)	1.37[a] (1.04-1.69)	1.76[a] (1.02-2.50)	-	-
GSTM3	-	-	-	-	-
HMOX1	-	-	-	1.46[a] (1.19-1.73)	1.79[a] (1.56-2.01)
MT2A	1.28[b] (1.02-1.54)	-	1.30[a] (1.09-1.50)	1.34[a] (1.15-1.53)	1.37[a] (1.12-1.61)
POR	1.28[a] (1.13-1.43)	-	-	-	-
PRDX1	1.28[b] (1.01-1.55)	1.42[a] (1.09-1.76)	1.23[b] (1.01-1.46)	-	-
PRDX2		1.29[a] (1.03-1.54)	-	-	-
PTGS1	-	-	-	1.37[a] (1.16-1.58)	1.21[a] (1.04-1.39)
SOD1	-	-	-	-	-
SOD2	-	-	-	-	-

[a]P<0.050, [b]P<0.056. CI, confidence interval.

3:1 (WHO fibres). Chrysotile has a curly, pliable structure with nearly equal magnesium (Mg)/silicon (Si) distribution (Fig. 2).

Irregularly shaped crystalline titanium dioxide aggregates (diameter, 1-3 μm) were observed (Fig 3). The micro-sized aggregates were composed of ~20 primary particles with a diameter between 100 and 200 nm. The specific surface (BET) of titanium dioxide was 9.9 m^2/g. Evaluation of the BET (for titanium dioxide and zirconium dioxide) was performed by K.-P- Company for surface- and solid state analysis mbH (o.f.u), Hamburg, Germany (Report B0104014 for the Federal Institute of Occupational Safety and Medicine, May 2001).

For zirconium dioxide, an aggregate diameter of 1-2 μm was determined. The crystalline aggregates were composed

Table IV. Comparing mRNA expression (95% CI) of DNA growth arrest and senescence molecules.

Growth arrest and senescence	Crocidolite fold change (95% CI)	Chrysotile fold change (95% CI)	Titanium dioxide fold change (95% CI)	Zirconium dioxide fold change (95% CI)	Hematite fold change (95% CI)
CDKN1A					
DDIT3	1.30[a] (1.02-1.57)	1.30[a] (1.02-1.57)	1.40[a] (1.02-1.57)	-	-
GADD45A	1.46[a] (1.11-1.80)	-	-	-	-
GDF15	1.41[a] (1.13-1.69)	-	-	-	-
IGFBP6	-	1.30[a] (1.13-1.69)	-	-	-
MDM2	-	-	-	-	-
TP53	1.19[a] (1.02-1.35)	-	-	-	-

[a]P<0.050. CI, confidence interval.

Table V. Comparing mRNA expression (95% CI) of inflammatory molecules.

Inflammation	Crocidolite fold change (95% CI)	Chrysotile fold change (95% CI)	Titanium dioxide fold change (95% CI)	Zirconium dioxide fold change (95% CI)	Hematite fold change (95% CI)
CCL21					
CCL3	2.05[a] (1.34-2.77)	3.16[a] (1.47-4.85)	2.79[a] (1.63-3.94)	-	-
CCL4	-	-	-	-	-
CSF2	1.54[a] (1.28-1.80)	-	-	-	1.54[a] (1.20-1.88)
CXCL10	-	-	-	-	-
IL18	-	-	-	-	-
IL1A	1.34[a] (1.09-1.59)	-	-	-	-
IL1B	1.39[a] (1.30-1.47)	-	-	-	-
IL6	1.76[a] (1.48-2.04)	1.59[a] (1.24-1.95)	-	-	1.53[a] (1.34-1.72)
LTA	-	-	-	-	-
MIF	-	1.35[a] (1.34-1.72)	-	-	-
NFKB1	-	-	-	-	-
NOS2	-	-	-	-	-
SERPINE1	1.45[a] (1.25-1.65)	1.42[a] (1.14-1.70)	-	-	1.45[a] (1.14-1.70)

[a]P<0.050. CI, confidence interval.

of ~50 primary particles with a diameter of ~100 nm (Fig. 4). The specific surface (BET) of zirconium dioxide was 5.9 m^2/g.

Hematite was found to be a spherical formed, nano-sized material. Agglomerates of 0.2-2 μm were formed by 50-500 primary particles with a diameter of ~20 nm. Additionally, smaller aggregates (<100 nm) were detected by electron microscopy (Fig. 5). The usually observed integration of water within the crystal lattice, caused by the production (precipitation) process of hematite, was excluded by TG (26-28).

After a 48-h exposure to the described fibres and particles, relative mRNA expression of 84 genes were determined four times. The average and standard deviation of the Ct values of each gene are shown in Table I.

Direct genotoxicity. Molecules of the 'DNA damage and repair' pathway were assigned to direct genotoxicity. In BEAS-2B cells, UGT1A4 mRNA expression could not be detected. mRNA expression of the 'DNA damage and repair' pathway was induced mainly by crocidolite, followed by chrysotile. Zirconium dioxide significantly upregulated UNG (1.31; P=0.043) but downregulated RAD50 (-1.45; P=0.038), while neither titanium dioxide nor hematite altered mRNA expression of 'DNA damage and repair' pathway signalling molecules (Table II).

Indirect genotoxicity. Molecules of the 'oxidative or metabolic stress', 'growth arrest and senescence' as well as 'inflammation' pathway were assigned to indirect genotoxicity. In BEAS-2B cells, Cyp7A1, FMO1, CCL21, CCL4, CXCL10 and LTA mRNA expression could not be detected. The majority of changes in the signalling molecule mRNA expression of the 'oxidative or metabolic stress' pathway were due to crocido-

Table VI. Comparing mRNA expression (95% CI) of DNA proliferation and carcinogenesis molecules.

Proliferation and carcinogenesis	Crocidolite fold change (95% CI)	Chrysotile fold change (95% CI)	Titanium dioxide fold change (95% CI)	Zirconium dioxide fold change (95% CI)	Hematite fold change (95% CI)
CCNC					
CCND1	1.57[a] (1.28-1.87)	1.89[a] (1.33-2.44)	2.36[a] (1.33-2.44)	-	-
CCNG1	-	-	-	-	-
E2F1	-	-	-	-	-
EGR1	-	-	-	-	-
PCNA	-	-	-	-	-

[a]P<0.050. CI, confidence interval.

Table VII. Comparing mRNA expression (95% CI) of heat shock molecules.

Heat shock	Crocidolite fold change (95% CI)	Chrysotile fold change (95% CI)	Titanium dioxide fold change (95% CI)	Zirconium dioxide fold change (95% CI)	Hematite fold change (95% CI)
DNAJA1	1.17[a] (1.03-1.31)	-	-	-	-
DNAJB4	-	-	-	-	-
HSF1	-	1.31[a] (1.05-1.56)	1.29[a] (1.14-1.44)	-	1.57[a] (1.33-1.81)
HSPA1A	1.30[a] (1.10-1.51)	-	1.22[a] (1.05-1.38)	1.25[a] (1.06-1.44)	-
HSPA1L	1.25[a] (1.05-1.46)	1.36[a] (1.13-1.60)	1.43[a] (1.21-1.64)	-	-
HSPA2	-	-	-	-	-
HSPA4	-	-	-	-	-
HSPA5	1.63[a] (1.21-2.04)	1.67[a] (1.07-2.27)	2.02[a] (1.37-2.67)	-	1.81[a] (1.25-2.36)
HSPA6	-	-	1.68[b] (0.83-2.53)	-	-
HSPA8	1.19[a] (1.09-1.28)	1.19[b] (1.02-1.35)	-	-	-
HSPB1	-	-	-	-	1.22[a] (1.09-1.34)
HSP90AA2	1.20[a] (1.03-1.37)	-	1.54[a] (1.10-1.98)	-	1.86[a] (1.44, 2.28)
HSP90AB1	-	-	-	-	1.19[a] (1.05-1.32)
HSPD1	-	1.40[a] (1.18-1.62)	-	-	1.23[a] (1.03-1.43)
HSPE1	-	-	-	-	1.36[a] (1.02-1.69)
HSPH1	-	-	1.47[a] (1.12-1.82)	-	1.41[a] (1.15-1.68)

[a]P<0.050, [b]P<0.058. CI, confidence interval.

lite. Notably, changes in signalling molecule expression were comparable for chrysotile, zirconium dioxide, titanium dioxide and hematite (Table III).

Both fibres showed a moderate increase in signalling molecule expression of the 'growth arrest and senescence' pathway, while titanium dioxide only induced DDIT3 (1.4, P=0.048). There was no significant change in mRNA expression due to zirconium dioxide and hematite (Table IV).

Molecules belonging to the 'inflammation' pathway were induced mainly by crocidolite. Chrysotile and hematite provoked a comparable moderate increase in gene expression. Titanium dioxide distinctly induced CCL3 (2.79, P=0.007), while there were no expression changes due to zirconium dioxide (Table V).

Initiation and promotion of carcinogenesis. Molecules of the 'proliferation and carcinogenesis' pathway were assigned to initiation and promotion of carcinogenesis. The only gene of this pathway, which was induced was Cyclin D1 (CCND1). Cyclin D expression was induced by crocidolite (1.57, P=0.004), chrysotile (1.89, P=0.019) and titanium dioxide (2.36, P=0.007) (Table VI).

Acute toxicity and/or genotoxicity. Molecules of the 'heat shock' and 'apoptosis' pathways were assigned to acute toxicity and/or genotoxicity. Of all investigated pathways, the greatest changes were found within these two pathways. Crocidolite, titanium dioxide and hematite provoked the most changes in mRNA expression of signalling molecules of the

Table VIII. Comparing mRNA expression (95% CI) of apoptosis molecules.

Apoptosis	Crocidolite fold change (95% CI)	Chrysotile fold change (95% CI)	Titanium dioxide fold change (95% CI)	Zirconium dioxide fold change (95% CI)	Hematite fold change (95% CI)
ANXA5	-	1.55[b] (1.01-2.08)	-	-	-
BAX	1.29[a] (1.05-1.53)	1.36[b] (1.00-1.72)	-	-	-
BCL2L1	1.66[a] (1.30-2.03)	-	-	-	-
CASP1	1.35[b] (1.11-1.58)	1.44[a] (1.07-1.81)	1.32[a] (1.02-1.61)	1.46[a] (1.21-1.70)	-
CASP10	-	-	-	-	-
CASP8	1.84[a] (1.22-2.45)	1.87[b] (1.01-2.73)	-	-	-
FASLG	-	-	-	-	-
NFKBIA	-	-	1.31[a] (1.06-1.57)	1.50[a] (1.21-1.78)	1.47[a] (1.15-1.79)
TNF	-	-	-	-	-
TNFRSF1A	-	-	-	1.42[a] (1.02-1.69)	-
TNFSF10	-	-	-1.29[c] [-1.11-(-1.45)]	-	-

[a]P<0.050, [b]P<0.059 and [c]P=0.038. CI, confidence interval.

Table IX. Comparison of induced signalling pathways by investigated particles.

	Direct genotoxicity	Indirect genotoxicity			Initiation and promotion of carcinogenesis	Acute toxicity and/or genotoxicity	
	DNA damage and repair	Oxidative or metabolic stress	Growth arrest and senescence	Inflammation	Proliferation and carcinogenesis	Heat shock	Apoptosis
Crocidolite	XX	XX	X	XX	(X)	XX	XX
Chrysotile	X	X	X	X	(X)	X	(X)
TiO_2 Anastas	-	X	(X)	(X)	(X)	XX	X
ZrO_2	(X)	X	-	-	-	(X)	XX
Hematite	-	X	-	X	-	XX	(X)

XX, high mRNA-induction; X, moderate mRNA-induction; (X), low mRNA-induction; TiO_2, titanium dioxide; ZrO_2, zirconium dioxide.

'heat shock' pathway, while crocidolite and zirconium dioxide provoked the most changes in mRNA expression of signalling molecules of the 'apoptosis pathway'. Chrysotile showed a moderate increase of 'heat shock' genes and only a moderate increase of 'apoptosis' genes (Tables VII and VIII).

A comparison of the pathways induced by crocidolite, chrysotile, titanium dioxide, zirconium dioxide and hematite is provided in Table IX.

Discussion

In this study, we compared the ability of two different fibres (crocidolite and chrysotile) and three different sized particles (titanium dioxide, zirconium dioxide and hematite) to induce the mRNA expression of signalling molecules involved in diverse pathways. We characterized the toxicologically relevant chemical and physical properties of the fibres and particles to ensure the comparability of the present results. UICC crocidolite South African and UICC chrysotile 'A' are asbestos fibres, and their cytotoxic and genotoxic potential is well studied. The selected bio-persistent dust particles, titanium dioxide (100-200 nm) and zirconium dioxide (50-100 nm), were of the same origin as formerly used *in vivo* (29). After intratracheal installation, both particles induced lung tumours in female SPF Wistar rats (29). Hematite (20 nm), the smallest of all particles, was investigated, to observe whether the obtained reaction may be provoked by the iron content.

Asbestos fibres caused the most relevant changes in gene expression of all tested pathways. This finding is in accordance with the general knowledge that crocidolite as well as chrysotile are asbestos fibres with a high cytotoxic and genotoxic effect (2,20,21,30,31). A literature search, including *in vitro* analysis, animal experiments and epidemiological studies, confirmed that all fibre types show comparable harmful effects (32). Chrysotile is, due to its higher solubility, less bio-persistent than the crocidolite (33). Since our study determines the early effects (48 h) of fibres and particles, the 5-year clearance rate is of minor relevance to our results. In accordance with our study, it appears that chrysotile and crocidolite

develop their genotoxicity due to direct and indirect (inflammatory driven) molecular mechanisms (18,19,34-36).

The iron content appears to not to be of major relevance for the observed induction of direct genotoxicity or the initiation and promotion of carcinogenesis, since these pathways are not induced by hematite (Fe 70%) but by zirconium dioxide (Fe 0%). In a study by Schürkes *et al*, the iron content appeared not to be relevant for the induction of 8-hydroxydeoxyguanosine (8-OHdG), since fibres with different iron amounts (0.025-20%) revealed comparable results (35). In the present study, nano-sized hematite and titanium dioxide showed an inflammatory and oxidative stress response and a high increase in gene expression attributed to the 'heat shock' pathway. These findings are in accordance with the results of Park *et al*, where single intratracheal instillation of iron nanoparticles (NP) in mice elevated the expression of many genes related to inflammation or tissue damage, such as heat shock proteins (37). Additionally, significant generation of ROS was described for titanium dioxide-NP and hematite (9,24,38). None of the investigated genes of the 'DNA damage and repair' pathway were induced by hematite or titanium dioxide in our study. Nanoparticles of hematite but not those of titanium dioxide induced significant DNA-breakage, measured by the Comet-assay in IMR-90 cells. DNA-damage and cytotoxic effects by hematite in BEAS-2B cells were not observed until a concentration of 50 $\mu g/cm^2$ was used (9). On the contrary to ultrafine titanium dioxide, there were no significant alterations in micronuclei induction by fine titanium dioxide observed in Syrian hamster embryo cells (23). Incorporation into human lung cells was described for fine and ultrafine titanium dioxide as well as for hematite (24,39).

Notably, Cyclin D1 which, as a regulatory subunit of CDK4 or CDK6, promotes cell cycle progression through G1-phase is significantly upregulated by titanium dioxide (relative expression 2.36) correspondingly with chrysotile (relative expression 1.89) and crocidolite (relative expression 1.57). The deregulation of cyclin D1 plays an important role in tumorigenesis and has frequently been linked to various types of human cancer (40).

Zirconium dioxide with particle sizes between 50 and 100 nm induced molecules attributed to the 'oxidative or metabolic stress' pathway, which suggests an indirect genotoxicity. We also found a high increase of apoptotic molecules. Zirconium dioxide induced UNG, which eliminates uracil from DNA molecules by cleaving the N-glycosylic bond and initiates the base-excision repair (BER) pathway. Uracil appearing in DNA, for example as a result of cytosine deamination, is potentially mutagenic and deleterious for cell regulation (41).

In particular, properties such as size, geometry, chemical composition and surface behaviour of particles play important roles in interaction with cells and modify their pathogenicity. Many published studies are missing detailed information on properties and the concentration of the particles used, which makes it difficult to compare results.

Our study and recent reports in the literature demonstrate that gene expression profiling in human lung epithelial cells can be an important tool for analyzing the pathogenicity of potentially harmful fibres and particles (42-44). Gene expression profiling, for example in response to asbestos, is valuable to define early molecular effects as demonstrated in diverse human cells, such as normal human bronchial epithelial cells (NHEC) (45), human lung adenocarcinoma cells (A549) (46,47), SV40-transformed human bronchial epithelial cells (BEAS-2B) and SV40-immortalized pleural mesothelial cells (MET5A) (47). Changes in gene expression are also valuable to determine the pathogenicity pathway of asbestos fibres, as demonstrated in the human mesothelial (LP9/TERT-1) cell line (42).

In further studies, new particles can be screened to complete the toxicological knowledge on the molecular effects and to assess potentially hazardous risks. Altogether, analysis of gene expression profiles may play an important role in the early detection of fibres or potential hazards of particles to human health.

Acknowledgements

This study was supported by the E.W. Baader-Stiftung supervised by the German Stiftungszentrum, Barkhovenallee 1, 45239 Essen, Germany, Az. T007/20368/2010/sm.

References

1. DFG: List of MAK and BAT Values 2011. Wiley-VCH Verlag GmbH & Co. KGaA, Weinheim, 2011.
2. Mossman BT, Bignon J, Corn M, Seaton A and Gee JB: Asbestos: scientific developments and implications for public policy. Science 247: 294-301, 1990.
3. Kamp DW: Asbestos-induced lung diseases: an update. Transl Res 153: 143-152, 2009.
4. Shukla A, MacPherson MB, Hillegass J, Ramos-Nino ME, Alexeeva V, Vacek PM, Bond JP, Pass HI, Steele C and Mossman BT: Alterations in gene expression in human mesothelial cells correlate with mineral pathogenicity. Am J Respir Cell Mol Biol 41: 114-123, 2009.
5. Lemaire I and Ouellet S: Distinctive profile of alveolar macrophage-derived cytokine release induced by fibrogenic and nonfibrogenic mineral dusts. J Toxicol Environ Health 47: 465-478, 1996.
6. Robledo R and Mossman B: Cellular and molecular mechanisms of asbestos-induced fibrosis. J Cell Physiol 180: 158-166, 1999.
7. Mossman BT and Churg A: Mechanisms in the pathogenesis of asbestosis and silicosis. Am J Respir Crit Care Med 157: 1666-1680, 1998.
8. Kamp DW and Weitzman SA: The molecular basis of asbestos induced lung injury. Thorax 54: 638-652, 1999.
9. Bhattacharya K, Davoren M, Boertz J, Schins RP, Hoffmann E and Dopp E: Titanium dioxide nanoparticles induce oxidative stress and DNA-adduct formation but not DNA-breakage in human lung cells. Part Fibre Toxicol 6: 17, 2009.
10. Hext PM, Tomenson JA and Thompson P: Titanium dioxide: inhalation toxicology and epidemiology. Ann Occup Hyg 49: 461-472, 2005.
11. Bernard BK, Osheroff MR, Hofmann A and Mennear JH: Toxicology and carcinogenesis studies of dietary titanium dioxide-coated mica in male and female Fischer 344 rats. J Toxicol Environ Health 29: 417-429, 1990.
12. Hart GA and Hesterberg TW: In vitro toxicity of respirable-size particles of diatomaceous earth and crystalline silica compared with asbestos and titanium dioxide. J Occup Environ Med 40: 29-42, 1998.
13. Gurr JR, Wang AS, Chen CH and Jan KY: Ultrafine titanium dioxide particles in the absence of photoactivation can induce oxidative damage to human bronchial epithelial cells. Toxicology 213: 66-73, 2005.
14. Kang SJ, Kim BM, Lee YJ and Chung HW: Titanium dioxide nanoparticles trigger p53-mediated damage response in peripheral blood lymphocytes. Environ Mol Mutagen 49: 399-405, 2008.
15. DaNa: Zirconium dioxide. http://nanopartikel.info/cms/lang/en/Wissensbasis/Zirkoniumdioxid. Accessed October 8, 2013.

16. NanoCare Project Partners: NanoCare. Health Related Aspects of Nanomaterials. Final Scientific Report. T.A.J. Kuhlbusch, H.F. Krug and K. Nau (eds). 1st edition. DECHEMA e.V. (in cooperation with the NanoCare Project Consortium), Frankfurt am Main, 2009.
17. Schneider J, Walter D, Brückel B and Rödelsperger K: Primary particles and their agglomerate formation as modifying risk factors of nonfibrous nanosized dust. J Toxicol Environ Health A 76: 131-141, 2013.
18. Dopp E, Schuler M, Schiffmann D and Eastmond DA: Induction of micronuclei, hyperdiploidy and chromosomal breakage affecting the centric/pericentric regions of chromosomes 1 and 9 in human amniotic fluid cells after treatment with asbestos and ceramic fibers. Mutat Res 377: 77-87, 1997.
19. Burmeister B, Schwerdtle T, Poser I, Hoffmann E, Hartwig A, Müller WU, Rettenmeier AW, Seemayer NH and Dopp E: Effects of asbestos on initiation of DNA damage, induction of DNA-strand breaks, P53-expression and apoptosis in primary, SV40-transformed and malignant human mesothelial cells. Mutat Res 558: 81-92, 2004.
20. Dopp E, Yadav S, Ansari FA, Bhattacharya K, von Recklinghausen U, Rauen U, Rödelsperger K, Shokouhi B, Geh S and Rahman Q: ROS-mediated genotoxicity of asbestos-cement in mammalian lung cells in vitro. Part Fibre Toxicol 2: 9, 2005.
21. Poser I, Rahman Q, Lohani M, Yadav S, Becker HH, Weiss DG, Schiffmann D and Dopp E: Modulation of genotoxic effects in asbestos-exposed primary human mesothelial cells by radical scavengers, metal chelators and a glutathione precursor. Mutat Res 559: 19-27, 2004.
22. Bhattacharya K: Comparative analysis of fine and nanoparticles for cellular uptake, oxidative stress and genomic damage in human lung cells (unpublished PhD thesis). University of Duisburg-Essen, 2009.
23. Rahman Q, Lohani M, Dopp E, Pemsel H, Jonas L, Weiss DG and Schiffmann D: Evidence that ultrafine titanium dioxide induces micronuclei and apoptosis in Syrian hamster embryo fibroblasts. Environ Health Perspect 110: 797-800, 2002.
24. Bhattacharya K, Hoffmann E, Schins RF, *et al*: Comparison of micro- and nanoscale Fe^{+3}-containing (Hematite) particles for their toxicological properties in human lung cells in vitro. Toxicol Sci 126: 173-182, 2012.
25. Pfaffl MW: A new mathematical model for relative quantification in real-time RT-PCR. Nucleic Acids Res 29: e45, 2001.
26. Buxbaum G and Paff G (eds): Industrial Inorganic Pigments. 3rd edition. Wiley-VCH Verlag GmbH & Co. KGaA, Weinheim, 2005.
27. Buxbaum G and Printzen H: Ullmann's Encyclopedia of Industrial Chemistry. Vol A20. 5th edition. VCH Verlagsgesellschaft mbH, Weinheim, p297, 1992.
28. Walter D: Characterization of synthetic hydrous hematite pigments. Thermochimica Acta 445: 195-199, 2006.
29. Pott F and Roller M: Carcinogenicity study with nineteen granular dusts in rats. Eur J Oncol 10: 249-281, 2005.
30. Jones JSP, Smith PG, Pooley FD, *et al*: Biological effects of mineral fibres. In: IARC Monographs on the Evaluation of Carcinogenic Risks to Humans. WHO International Agency for Research on Cancer, Lyon, pp637-653, 1980.
31. WHO, IARC: IARC Monographs on the Evaluation of Carcinogenic Risks to Humans Overall Evaluations of Carcinogenicity: An Updating of IARC Monographs Volumes 1 to 42. Supplement 7. IARC, Lyon, 1987. http://monographs.iarc.fr/ENG/Monographs/suppl7/suppl7.pdf. Accessed October 8, 2013.
32. Baur X, Schneider J, Woitowitz HJ and Velasco Garrido M: Do advers health effects of chrysotile and amphibole asbestos differ? Pneumologie 66: 497-506, 2012 (In German).
33. Bernstein DM, Rogers R and Smith P: The biopersistence of Canadian chrysotile asbestos following inhalation. Inhal Toxicol 15: 1247-1274, 2003.
34. Dopp E, Poser I and Papp T: Interphase fish analysis of cell cycle genes in asbestos-treated human mesothelial cells (HMC), SV40-transformed HMC (MeT-5A) and mesothelioma cells (COLO). Cell Mol Biol (Noisy-le-grand) 48: OL271-OL277, 2002.
35. Schürkes C, Brock W, Abel J and Unfried K: Induction of 8-hydroxydeoxyguanosine by man made vitreous fibres and crocidolite asbestos administered intraperitoneally in rats. Mutat Res 553: 59-65, 2004.
36. Ruosaari S, Hienonen-Kempas T, Puustinen A, Sarhadi VK, Hollmén J, Knuutila S, Saharinen J, Wikman H and Anttila S: Pathways affected by asbestos exposure in normal and tumour tissue of lung cancer patients. BMC Med Genomics 1: 55, 2008.
37. Park EJ, Kim H, Kim Y, Yi J, Choi K and Park K: Inflammatory responses may be induced by a single intratracheal instillation of iron nanoparticles in mice. Toxicology 275: 65-71, 2010.
38. Könczöl M, Ebeling S, Goldenberg E, Treude F, Gminski R, Gieré R, Grobéty B, Rothen-Rutishauser B, Merfort I and Mersch-Sundermann V: Cytotoxicity and genotoxicity of size-fractionated iron oxide (magnetite) in A549 human lung epithelial cells: role of ROS, JNK, and NF-kappaB. Chem Res Toxicol 24: 1460-1475, 2011.
39. Singh S, Shi T, Duffin R, Albrecht C, van Berlo D, Höhr D, Fubini B, Martra G, Fenoglio I, Borm PJ and Schins RP: Endocytosis, oxidative stress and IL-8 expression in human lung epithelial cells upon treatment with fine and ultrafine TiO_2: role of the specific surface area and of surface methylation of the particles. Toxicol Appl Pharmacol 222: 141-151, 2007.
40. Witzel, II, Koh LF and Perkins ND: Regulation of cyclin D1 gene expression. Biochem Soc Trans 38: 217-222, 2010.
41. Zharkov DO, Mechetin GV and Nevinsky GA: Uracil-DNA glycosylase: structural, thermodynamic and kinetic aspects of lesion search and recognition. Mutat Res 685: 11-20, 2010.
42. Hillegass JM, Shukla A, MacPherson MB, Bond JP, Steele C and Mossman BT: Utilization of gene profiling and proteomics to determine mineral pathogenicity in a human mesothelial cell line (LP9/TERT-1). J Toxicol Environ Health A 73: 423-436, 2010.
43. Perkins TN, Shukla A, Peeters PM, Steinbacher JL, Landry CC, Lathrop SA, Steele C, Reynaert NL, Wouters EF and Mossman BT: Differences in gene expression and cytokine production by crystalline vs. amorphous silica in human lung epithelial cells. Part Fibre Toxicol 9: 6, 2012.
44. Huang YC, Karoly ED, Dailey LA, Schmitt MT, Silbajoris R, Graff DW and Devlin RB: Comparison of gene expression profiles induced by coarse, fine, and ultrafine particulate matter. J Toxicol Environ Health A 74: 296-312, 2011.
45. Belitskaya-Levy I, Hajjou M, Su WC, Yie TA, Tchou-Wong KM, Tang MS, Goldberg JD and Rom WN: Gene profiling of normal human bronchial epithelial cells in response to asbestos and benzo(a)pyrene diol epoxide (BPDE). J Environ Pathol Toxicol Oncol 26: 281-294, 2007.
46. Hevel JM, Olson-Buelow LC, Ganesan B, Stevens JR, Hardman JP and Aust AE: Novel functional view of the crocidolite asbestos-treated A549 human lung epithelial transcriptome reveals an intricate network of pathways with opposing functions. BMC Genomics 9: 376, 2008.
47. Nymark P, Lindholm PM, Korpela MV, Lahti L, Ruosaari S, Kaski S, Hollmén J, Anttila S, Kinnula VL and Knuutila S: Gene expression profiles in asbestos-exposed epithelial and mesothelial lung cell lines. BMC Genomics 8: 62, 2007.